





Design and Simulation of Single-Mode and Polarization Independent Deeply Etched Amorphous Silicon on SOI Waveguides

Babak Hashemi¹^a, Sandro Rao¹^b, Maurizio Casalino²^c and Francesco Della Corte³^d

¹*Department of Information Engineering Infrastructures and Sustainable Energy (DIIES),*

“Mediterranea” University Reggio Calabria, Italy

²*Institute of Applied Sciences and Intelligent Systems (ISASI) National Research Council (CNR) Naples, Italy*

³*Department of Electrical Engineering and Information Technologies, Università degli Studi di Napoli Federico II, 80125 Naples, Italy*

Keywords: Polarization-Independent, Single-Mode, SOI Waveguides, Amorphous Silicon.


Abstract: The conditions for simulating both single-mode behavior and polarization independence in deeply etched amorphous silicon (a-Si) on Silicon-On-Insulator (SOI) rib waveguides are presented and discussed. The paper aims to provide valuable insights and guidance for the design and optimization of waveguide-integrated electro-optic devices based on deeply etched hydrogenated amorphous silicon (a-Si:H)/SOI waveguides operating in a broad spectrum of wavelengths. The top layer of the waveguide consists of a-Si:H, whose deposition can be performed at low temperatures with no impact at all for previously fabricated CMOS-based electro-photonic integrated circuit.


1 INTRODUCTION


The rapid evolution of photonic technologies has ushered in a new era of high-speed data communication, sensing, and signal processing (Marpaung, Yao, & Capmany, 2019). Among the many facets of integrated-waveguide design, achieving both single-mode behavior and polarization independence stands as a complex challenge, however pivotal to a variety of photonic applications (Aalto, et al., 2019), (Lim, Eng Png, Ong, & Ang, 2007). To date, many studies have been conducted; e.g., Neslihan and Kurt (Neslihan & Kurt, 2016) analyzed the mode characteristics and light confinement properties of different geometries of rib waveguides, Seong et al. (Seong P., Eng Png, & Lim, 2004) investigated polarization-independent SOI waveguides giving valuable insights into the requirements for achieving such condition. More recently, SM (single-mode) and PI (polarization-independent) waveguides play a pivotal role in different devices. A proposed power splitter utilizes


these features with three waveguides (Samanta, Dey, Banerji, & Ganguly, 2018), while (Zhang, et al., 2020) explores the design of a hybrid-plasmonic-waveguide directional coupler.

In this paper, we explore the design and simulation of single-mode (SM) and polarization-independent (PI) large cross-section waveguides, focusing on deeply etched a-Si:H/SOI rib waveguides. The introduction of a-Si:H material deposited as a back-end process of the standard CMOS-based fabrication, ensures, in principle, a full compatibility with existing microelectronics and photonics leading to new integrated photonic architecture with new functionalities in a wide range of applications. a-Si:H can be, in fact, deposited at relatively low temperatures ($T < 150^\circ\text{C}$), a property that has opened up the way for a true integration of photonics and electronics without any risks to existing CMOS devices (Della Corte & Rao, 2013) (Spear & Le Comber, 1975).

^a <https://orcid.org/0000-0003-4851-5639>

^b <https://orcid.org/0000-0001-8485-5046>

^c <https://orcid.org/0000-0003-2331-4419>

^d <https://orcid.org/0000-0002-2407-2979>

Moreover, the requirement of waveguides, satisfying both SM and PI behavior, has significant relevance in the design of photonic integrated circuits (PICs) as electro-optic (EO) modulators (Ma, Li, Han, Maeda, & Pištora, 2021), passive and active switches for telecommunications, and similar.

2 THEORETICAL SCHEME

A waveguide propagating mode has an effective refractive index that can be defined as follows (Jia-Ming, 2009):

$$k_z = n_{eff} \frac{2\pi}{\lambda} \quad (1)$$

Where k_z is value (phase constant) of the waveguide,

n_{eff} is the effective refractive index and λ is the wavelength.

The effective refractive index provides insight into how tightly the mode is confined within the waveguide core. For guided modes, the effective index should satisfy the following condition:

$$n_{clad} < n_{eff} < n_{core}.$$

For unguided or radiating modes (Butt & Kozlova, 2017):

$$n_{eff} < n_{clad}.$$

Therefore, modes are supported to the waveguide-core propagation only if their effective index is larger than the refractive index of the slab. Moreover, the effective index calculation can also be explored to determine the waveguide geometries for designing PI waveguides. To achieve this last condition, the effective index values of fundamental TE- and TM-polarized light must be equal. (Dai, Liu, Gao, Xu, & He, 2013)

3 SM AND PI WAVEGUIDE DESIGN

The structure under consideration is a rib waveguide consisting of three different layers: SiO₂ (cladding layer), crystal silicon (c-Si) and a-Si:H (core layers), as showed schematically in Fig. 1.

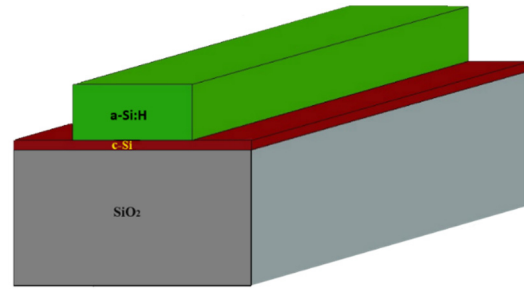


Figure 1: Schematic cross-section waveguide structure

Table 1: Layer geometries and physical parameters.

	Height	Width	Length	Refractive Index
SiO ₂	3 μm	3 μm	50 μm	1.44
Crystal Silicon	220nm	3 μm	50 μm	3.47
amorphous Silicon	h	w	50 μm	3.57

Ansys Lumerical Photonic Multiphysics Simulation tool (Bachorec & Sedlář, 2018) has been used for numerical calculations, providing geometries and physical material parameters for each layer considered, as reported in Table 1. First, the waveguide length was fixed to L=50 μm.

The optimal performance of semiconductor devices is considered while determining the 220 nm thickness of crystalline silicon (c-Si) in CMOS wafers (Bellutti, Boscardin, Soncini, Zen, & Zorzi, 1995). This thickness was chosen after thorough consideration of all the factors of the optical device, aiming to achieve optimal performance in both the optical and electrical domains. The aim of this first run of parametric simulations is to calculate the ideal height (h) and width (w) for the a-Si:H layer to achieve both criteria of SM behavior and PI.

4 SIMULATION RESULT

4.1 Single-Mode Condition

Parametric simulations have been performed to calculate the difference between the effective index of the modes propagating into the a-Si:H waveguide core and the refractive index of the thin layer of c-Si (nc-Si = 3.47). Fig. 2 shows the corresponding results, at the wavelength of 1.55 μm, as a function of the a-Si:H height. If a waveguide width of W=1.5 μm is considered, the SM condition can be achieved for an a-Si:H height ranging from 0.8 μm up to 2 μm. Beyond these values, high-order modes appear.

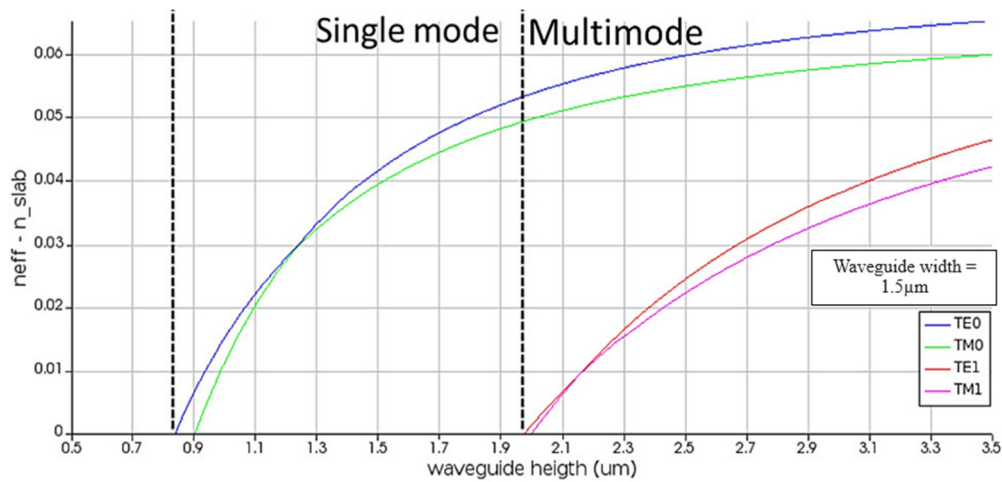


Figure 2: Effective refractive index difference between the waveguide-core propagating optical modes and refractive index of the c-Si as a function of the amorphous silicon height.

4.2 Polarization Independent (PI) Waveguide

In Fig. 3, the effective refractive index of the fundamental TE-polarized optical field is subtracted from the effective index of the fundamental TM mode as a function of the a-Si:H height, always considering a constant value for the a-Si:H width ($W = 1.5 \mu\text{m}$) at the wavelength of 1550 nm.

The a-Si:H height (h) that results in Δn equal to zero is determined to be $1.22 \mu\text{m}$ about.

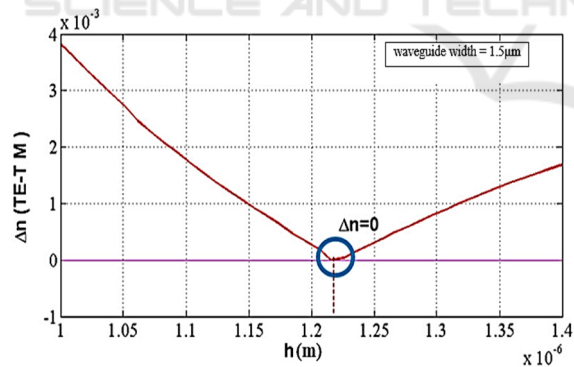


Figure 3: Difference between the effective refractive index of TE and TM modes (Δn) as a function of the amorphous silicon height.

4.3 Polarization Independent and Single Mode Waveguide

To achieve both PI and SM conditions for different cross-section waveguide geometries, parametric simulations were performed for all of the combinations of height (h) and width (w) of a-Si:H at

a fixed wavelength, as shown in Fig. 4. The achieved results were used to identify the overlapping region that meets both criteria.

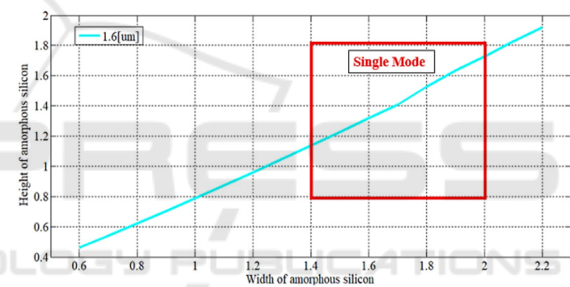


Figure 4: a-Si:H height as a function of width. Both PI and SM conditions are achieved in the range $1.4 \mu\text{m} < W_{\text{a-Si:H}} < 2 \mu\text{m}$ at the wavelength of $1.6 \mu\text{m}$.

In order to extend the operating wavelengths beyond the fiber-optic window, parametric simulations were performed for wavelengths ranging from $\lambda = 1.2 \mu\text{m}$ to $1.6 \mu\text{m}$. Fig. 5 shows heights and widths of a-Si:H that simultaneously satisfy both PI and SM conditions. It is worth noting that if the width of a-Si:H is $W = 1.46 \mu\text{m}$ and the a-Si:H height falls in between $1.19 \mu\text{m}$ and $1.15 \mu\text{m}$, a SM and PI waveguide can be achieved throughout the considered wide wavelength window. The outcomes of this study not only offer valuable insights into the optimal geometric parameters of a-Si:H waveguides for specific operational conditions but also provide a pathway for enhancing their versatility across a wider range of wavelengths. These findings contribute to the ongoing efforts to advance the development of efficient and adaptable photonic devices for diverse applications in optical communication and beyond.

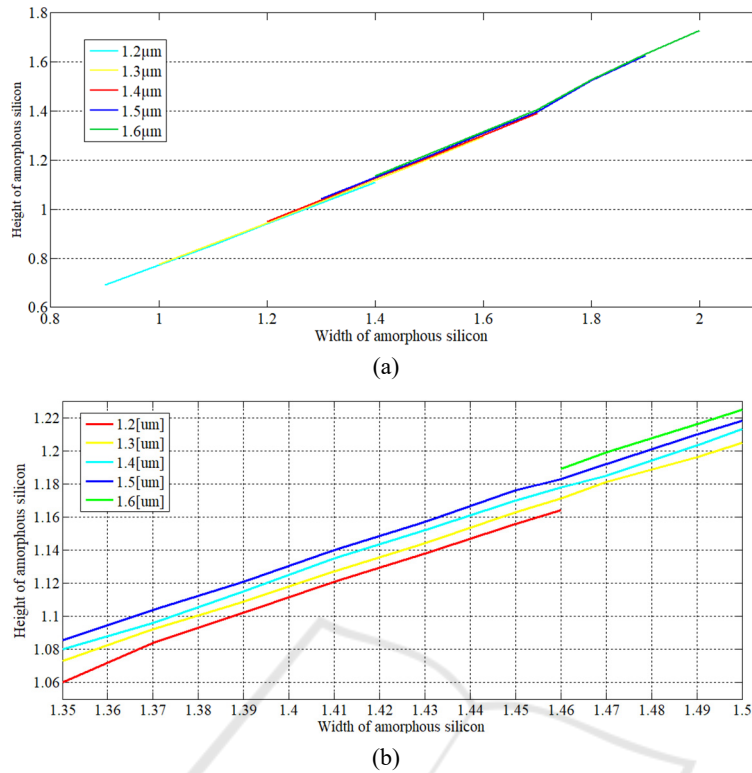


Figure 5: a-Si:H height (h) as a function of width for different wavelengths (a), in the range $0.9 \mu\text{m} < \text{Wa-Si:H} < 2 \mu\text{m}$ (b) in the range $1.35 \mu\text{m} < \text{Wa-Si:H} < 1.5 \mu\text{m}$.

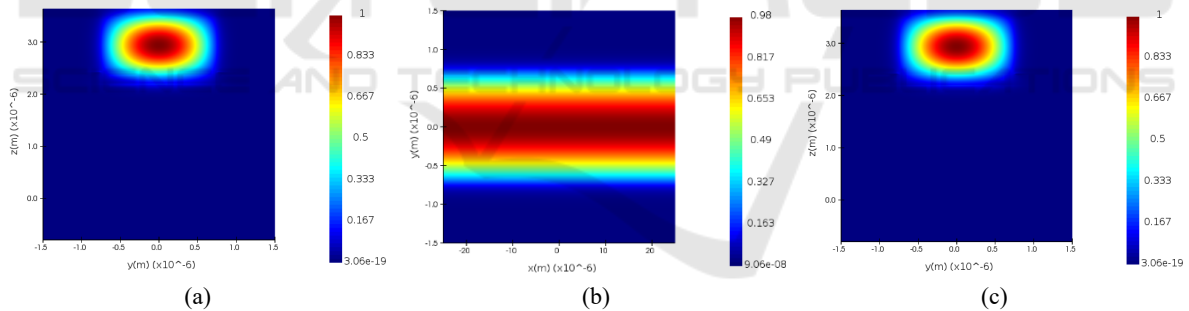


Figure 6: e-Field amplitude at the input (a), along the propagation direction (b) and at the waveguide output (c) for the PI and SM waveguide 3 mm-length at $\lambda = 1.5 \mu\text{m}$.

4.4 Waveguide with Longer Length

In Fig. 6, finite-difference time-domain (FDTD)-based simulation results about the propagation of the fundamental TE/TM mode along a SM and PI waveguide, $L=3 \text{ mm}$ long, are reported at various positions along the propagation direction.

Based on Figure 6, despite a substantial increase in the waveguide length, the guided mode propagating through it shows no significant losses. Consequently, it is reasonable to assume that the simulated single-mode (SM) and polarization-independent (PI) waveguide, characterized by a large

cross-sectional area, can be efficiently applied in the development of both passive and active devices even with extended length.

5 CONCLUSION

In this study, the design of single-mode and polarization-independent large cross-section waveguides have been investigated using commercial software. We successfully identified the optimal geometries to achieve both conditions in a wide operating wavelength range, from 1.2 up to 1.6 μm .

These results provide valuable insights to support the ongoing advancement of optical communications by developing new integrated electro-optic integrated devices to be explored in many application fields, from sensing to telecommunications.

ACKNOWLEDGMENT

Graphics project (F5) under the RESTART research program (PE-14) (MUR PE00000001) is acknowledged.

REFERENCES

- Aalto, T., Cherchi, M., Harjanne, M., Bhat, S., Heimala, P., Sun, F., . . . Vehmas, T. (2019). Open-access 3- μm SOI waveguide platform for dense photonic integrated circuits. *IEEE Journal of selected topics in quantum electronics*, 25(5), 1-9.
- Bachorec, T., & Sedlář, T. (2018). A new era in simulation. *IEEE*. Mikulov, Czech Republic.
- Bellutti, P., Boscardin, M., Soncini, G., Zen, M., & Zorzi, N. (1995). On the choice of the optimum silicon substrate for CCD/CMOS technology. *In Proceedings of 4th International Conference on Solid-State and IC Technology*, 176-178.
- Butt, M., & Kozlova, E. (2017). Single mode ZnO/Al₂O₃ Strip loaded waveguide at 633 nm visible wavelength. *Information technology and nanotechnology*.
- Dai, D., Liu, L., Gao, S., Xu, D.-X., & He, S. (2013). Polarization management for silicon photonic integrated circuits. *Laser & Photonics Reviews*, 7(3), 303-328.
- Della Corte, F. G., & Rao, S. (2013). Use of Amorphous Silicon for Active Photonic Devices. *IEEE Transactions on Electron Devices*, 1495-1505.
- Jia-Ming, L. (2009). *Photonic devices*. Cambridge University Press.
- Lim, S., Eng Png, C., Ong, E., & Ang, Y. (2007). Single mode, polarization-independent submicron silicon waveguides based on geometrical adjustments. *Optics Express*, 15(18), 11061-11072.
- Ma, Y., Li, J., Han, Z., Maeda, H., & Pištora, J. (2021). All-dielectric graphene-induced T-slot waveguide electro-optic modulator with polarization-independent operation. *IEEE Journal of Selected Topics in Quantum Electronics*, 27(3), 1-8.
- Marpaung, D., Yao, J., & Capmany, J. (2019). Integrated microwave photonics. *Nature photonics*, 13(2), 80-90.
- Neslihan, E., & Kurt, H. (2016). Model analysis of ridge and rib types of silicon waveguides with void compositions. *IEEE Journal of Quantum Electronics*, 52(10), 1-7.
- Samanta, S., Dey, P. K., Banerji, P., & Ganguly, P. (2018). A 1×2 polarization-independent power splitter using three-coupled silicon rib waveguides. *Journal of Optics*, 20(9), 095801.
- Seong P., C., Eng Png, C., & Lim, S. (2004). polarisation independent waveguides in silicon-on-insulator. *Ist IEEE International Conference on Group Iv Photonics*, 115-117.
- Spear, W., & Le Comber, P. (1975). Substitutional doping of amorphous silicon. *Solid state communications*, 17(9), 1193-1196.
- Zhang, L., Pan, C., Zeng, D., Yang, Y., Yang, Y., & Junxian, M. (2020). A Hybrid-Plasmonic-Waveguide-Based Polarization-Independent Directional Coupler. *IEEE Access*, 8, 134268-134275.